



**Theory and Simulation of Diffusion-Adsorption into
Molecularly Imprinted Mesoporous Film and Its
Nanostructured Counterparts. Experimental Application for
Trace Explosive Detection**

Journal:	<i>RSC Advances</i>
Manuscript ID:	RA-ART-07-2014-007000
Article Type:	Paper
Date Submitted by the Author:	11-Jul-2014
Complete List of Authors:	Zhu, Wei; Tsinghua University, Department of Chemistry Wang, Chen; Tsinghua University, Department of Chemistry Wang, Hui; Tsinghua University, Chemistry Li, Guangtao; Tsinghua University, Chemistry

ARTICLE

Theory and Simulation of Diffusion-Adsorption into Molecularly Imprinted Mesoporous Film and Its Nanostructured Counterparts. Experimental Application for Trace Explosive Detection

Cite this: DOI: 10.1039/x0xx00000x

Received 00th January 2012,
Accepted 00th January 2012

DOI: 10.1039/x0xx00000x

www.rsc.org/

Wei Zhu, Chen Wang, Hui Wang and Guangtao Li*

To better understand the complex problem of diffusion-adsorption of small gas molecules in molecularly imprinted porous (MIP) systems, two general and suitable physicomathematical models have been developed for the molecularly imprinted mesoporous film and its nanostructured counterparts. These theoretical and numerical formulations give a quantitative and general description of the complicated diffusion-absorption kinetic behavior of trace analyte in the MIP systems. These models show a strong dependence of the performance (sensitivity and selectivity) of the constructed chemosensors on their structure and imprinting efficiency, and provide the determined preparation factors to achieve high-performance chemosensors. As a demonstration, chemosensors based on the TNT-imprinted mesoporous films with P6mm structures were fabricated, and confirmed the validity and suitability of the physicomathematical models. Yet, these models may easily be modified and expanded to other research fields such as catalysis and separation.

Introduction

The development of porous materials with high surface areas and large specific pore volumes, particularly functionalized with specific functional groups, has been attracted great attentions during the past decades.¹⁻⁵ Among the various shapes and morphologies (powders, monoliths, fibers and films), thin films with meso- or hierarchical porous (MHP) structure are interesting and useful for versatile applications, particularly in chemical/gas sensors.⁶⁻⁹ Commonly, in such sensor applications, a careful selection of binding sites to decorate the pore surface with proper binding affinity and selectivity toward to the analytes and the optimization of the structure parameters (pore radius, pore length, etc.) to achieve an optimum pore structure are the two important aspects that determine the sensor performance (sensitivity and selectivity). For the first aspect, molecular imprinting (MI),¹⁰⁻¹² which is an established technique to create specific binding sites through careful selection of functional groups and shape recognition, has become a powerful method to modulate the pore surface properties. By generating the imprinted sites complementary to the shape, size and chemical functionality of the template, the selectivity toward to the analytes could be greatly improved. Recently, although molecular imprinting strategy has been exploited for many years, most of the reported works focus on the experimental investigations on imprinting efficiency.¹³⁻¹⁵ On the contrary, the theoretical and systematic studies on the modulation of molecular imprinting to gain deeper understand-

ing of the diffusion and adsorption behavior of gas molecules in imprinted mesochannels were still rare.

For the other aspect, optimizing the pore structure to achieve a good sensing performance is always the central part in sensor development. Currently, numerous studies have proved the relationship between the pore structure and sensing performance.¹⁶⁻¹⁹ In fact, small molecules diffusion in meso- or hierarchical porous films is a complex process. In these kinds of porous systems, the sensing performance is limited by a large series of factors, not only the pore structure (pore size, pore length, surface area, void volume), but also other factors such as the surface concentration and distribution of binding sites in the pore walls, the binding strength between the binding sites and analytes, etc. Evidently, there are so many parameters, and it is very hard to describe each factor from the experimental view. In this case, the creation of physicomathematical models would be a facile and feasible way to describe the diffusion-adsorption behaviors of analytes in these complex porous film systems. Up to now, numerous theoretical works have been performed in the nano- and mesoporous particle systems or conventional mesoporous films without specific binding sites.²⁰⁻³¹ For example, Amatore theoretically investigated the diffusion-reaction of small molecules into the former systems, where the model framework encompassed almost all situations of practical interest in solutions.²⁰⁻²² Bein and co-workers reported the single-molecule diffusion in the latter ordered mesoporous film system.²⁴⁻²⁵ However, the report on theoretical investigation of the influence of structural factors on the diffusion and adsorption behavior of gas molecules in

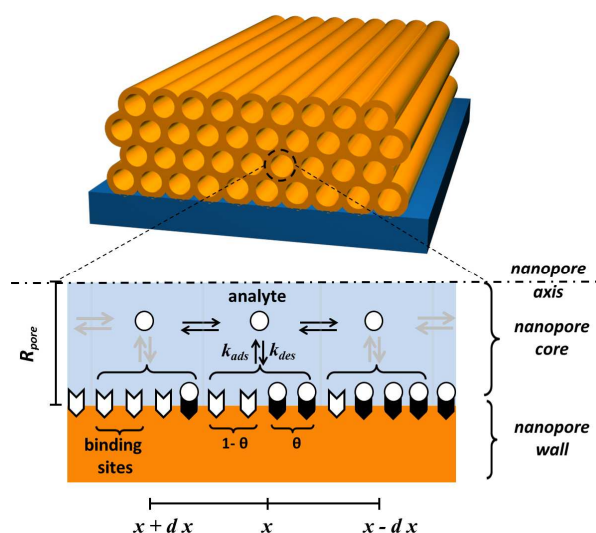


Figure 1. Schematic representation of the diffusion-adsorption process of analyte in the molecularly imprinted mesoporous film with p6mm structure.

imprinted film systems as well as the possible ways to modulate the sensor performance, especially the sensitivity and selectivity, has not been described.

In this work, to better understand the complex problem of diffusion-adsorption of small gas molecules in molecularly imprinted porous (MIP) film systems (Figure 1), two general and suitable physicomathematical models had been developed for the molecularly imprinted mesoporous film and its nanostructured counterparts. These theoretical and numerical formulations give a quantitative and general description of the complicated diffusion and absorption behavior of trace analyte in the MIP systems. In the first part, the validity and suitability of the physicomathematical model was proved by the experiments where trace explosive TNT and DNT detection was carried out in the TNT-imprinted mesoporous films with P6mm structure. Based on the simple curve fitting, some useful intrinsic parameters that were hardly determined by experiment were also derived. Moreover, we further explored the parameters (pore size, pore length, surface concentration and distribution of binding sites) on their ways to modulate the sensor sensitivity and also the parameters (the rate constants of chemical adsorption/desorption between the binding sites and analytes, and the imprinting efficiency) on their ways to control the selectivity. Based on the careful discussion, we found the parameters of pore length and the apparent rate constant of adsorption were the most important factors to influence the sensitivity and selectivity of sensor, respectively. After the optimization of both parameters, a sensor with good sensitivity and selectivity could be achieved. These developed models in our work offered us useful information and guideline for design and fabrication of chemosensors with improved performance. Yet, most importantly, these modes may easily be modified and expanded to other research fields such as catalysis and separation.

Experimental Section

Synthesis of TNT-imprinted organosilica precursor to form mesoporous films: 5 mg (8.80×10^{-3} mmol) Naphtalene-bridged silane (BTPN) and 1 mg (4.40×10^{-3} mmol) TNT were

dissolved in 2.93 ml anhydrous ethanol. After stirring at RT for 2 h, 3.54 g (10 mmol) 1,2-bis(trimethoxysilyl)ethane (BTME), 0.38 g (21 mmol) water and 12.3 μ l (0.07 M) HCl were added, and the resulting reaction mixture was refluxed at 60°C for 90 min. Then, 1.25 ml water and 65.4 μ l HCl (1M) were added for further 15 min stirring. The formed sol was further diluted with ethanol and mixed with non-ionic surfactant F127. The final molar ratio of the reactants was 1 BTME: 8.8×10^{-4} BTPN: 4.4×10^{-4} TNT: 217.6 EtOH: 9.1 H₂O: 6.5×10^{-3} HCl: 0.019 F127.

Synthesis of nonimprinted organosilica precursor to form mesoporous films: 5 mg (8.80×10^{-3} mmol) Naphtalene-bridged silane (BTPN) was dissolved in 2.93 ml anhydrous ethanol. After stirring at RT for 2 h, 3.54 g (10 mmol) BTME, 0.38 g (21 mmol) water and 12.3 μ l (0.07 M) HCl were added, and the resulting reaction mixture was refluxed at 60°C for 90 min. Then, 1.25 ml water and 65.4 μ l HCl (1M) were added for further 15 min stirring. The formed sol was further diluted with ethanol and mixed with non-ionic surfactant F127. The final molar ratio of the reactants was 1 BTME: 8.8×10^{-4} BTPN: 217.6 EtOH: 9.1 H₂O: 6.5×10^{-3} HCl: 0.019 F127.

Synthesis of organosilica precursor to form Macro-mesoporous films: 8.83 g (0.19 mol) anhydrous ethanol, 0.69 g (0.038 mol) water and 0.1 ml HCl (1 M) were mixed together, and then 0.46 g F127 was added to the solution. After the solution was clear, 1 g (4.81 mmol) TEOs and 5 mg (8.80×10^{-3} mmol) Naphtalene-bridged silane (BTPN) were added, and the resulting reaction mixture was refluxed at 80°C for 1 h. The final molar ratio of the reactants was 1 TEOs: 1.83×10^{-3} BTPN: 39.5 EtOH: 9.15 H₂O: 0.021 HCl: 7.59×10^{-3} F127. Before using, the formed sol was further diluted twice with ethanol.

Results and discussion

1. Experimental Results

Rapid detection and discrimination of hidden explosives are very important aspects concerning homeland security, environmental and humanitarian safety.³²⁻³⁶ In this task, in order to prove the validity and suitability of the constructed physicomathematical model, the experiments of trace explosive TNT and DNT detection were carried out in the TNT-imprinted mesoporous films with P6mm structure. For the imprinting process, thin films with meso- or hierarchical porous structures were prepared by the sol-gel deposition of imprinting-complex containing mesoporous silica material onto glass substrate or inside a colloidal crystal template separately. After the removal of all the used templates, the imprinted sites in MHP films were generated for selective sensing. The detail fabrication processes could be found in the experimental section. In the present case, naphthalene-bridged silane (BTPN) was synthesized as a functional monomer for the formation of TNT-imprinted complex, arising from strong charge-transfer interaction between electron-sufficient naphthalene and electron-deficient TNT.⁹ However, for the nonimprinted counterparts, BTPN was direct incorporation into silica matrix by co-condensation method to have a uniform functional group distribution inside the pore walls. As shown in Figure 2, the TEM images suggested that the pore channels in the mesoporous and macro-mesoporous films were well organized. BET analysis of N₂ adsorption-desorption experiments (Figure S1) yielded the mesoporous film with a specific surface area of 247 m²/g, a total pore volume of 0.34 cm³/g, a mean pore diameter (BJH method) of 5.6 nm and the macro-mesoporous film with a

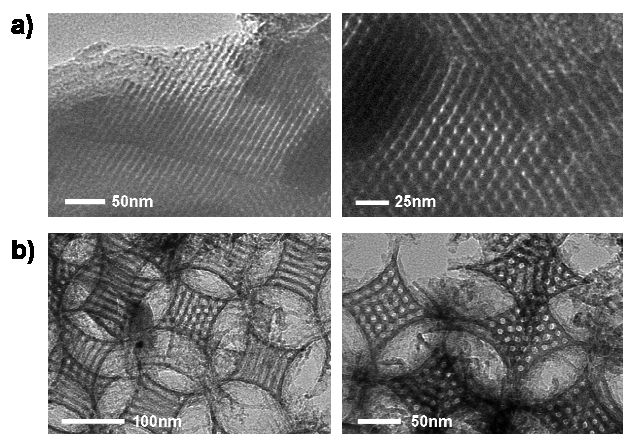


Figure 2. TEM images of (a) mesoporous and (b) the macro-mesoporous silica film after the extraction of all used templates.

specific surface area of 364 m²/g, a total pore volume of 0.58 cm³/g, and a mean pore diameter (BJH method) of 7.7 nm. Due to the low concentration of BTPN silane in the porous films, the doped amount was hard for determination by elemental analysis. Nevertheless, we can still get the concentration value by easily fitting the experimental curves.

The fluorescence response of the nonimprinted and imprinted mesoporous films to the vapors of nitro-containing aromatics (TNT or DNT) was ascertained by inserting the prepared films into glass vials (10 ml) at room temperature containing 1.5 g solid analytes and cotton gauze, which prevents the direct contact of silica film from analyte and helps to maintain a constant saturated vapor pressure. The analyte's equilibrium saturated vapor pressures are assumed to be similar to documented values (TNT: 10 ppb; DNT: 180 ppb). Fluorescence quenching experiments were performed to characterize the sensing rate. The quenching curves enabled us to monitor the diffusion-adsorption kinetics in the form of the variation of fluorescence quenching $Q(t)$ (defined as $(I_0 - I)/I_0$; I_0 : the original peak intensity). Considering that at each instant, $Q(t)$ was proportional to $\theta(t)$ (the average coverage of the binding sites in nanopore walls), it ensured the creation of the relationship between experiment and physicomathematical modeling.

Panels (a) and (b) in Figure 3 described the kinetic procedures as obtained where trace explosive TNT and DNT detection was operated in the TNT-imprinted or nonimprinted mesoporous films. As apparent from the two plots, the imprinting process afforded the films a preferred affinity to TNT and led to a remarkable increase of quenching efficiency of TNT over DNT, although the latter provide about 18 times higher vapor concentration. This selective sensing demonstrated that molecular imprinting was indeed a good strategy to modulate the rate constants of chemical adsorption and desorption between the analytes and binding sites to well control the sensor performance.

2. Theory and Simulation of the Experimental Systems

In this task, we would like to develop a general physicomathematical modeling to discuss the overall kinetic and thermodynamic behaviors inside the molecularly imprinted mesoporous films. This enabled us to extract the main factors that govern the system reactivity and direct us to achieve a higher-performance chemosensor.

Basically, several parameters controlled the sensing behavior.

For a clear delineation, in these systems, the parameters were divided into four groups: (i) the structure factor including the pore size and pore length, (ii) the distribution factor including the surface concentration of nonimprinted or imprinted sites and their corresponding distributions inside the pore wall surface, (iii) the combination strength factor including the rate constants of chemical adsorption/desorption between the binding sites and analytes, and (iv) the molecular imprinting factor including the regulatory factors to describe the molecular imprinting efficiency. Evidently, based on such a series of parameters, few of them were known, but there were still some other parameters that were hard to be determined by experimental characterizations. Nevertheless, one may still get them by easily fitting any smooth curves such as the experimental curves presented in.

In these systems, concentration gradient acted as the driving force, and then analytes diffused into the interior. During the detection process, it was assumed that the glass vials always kept a constant saturated vapor pressure. Based on this assumption, the concentration at the nanopore entrance could be considered as the bulk concentration. Simultaneously, co-condensation method was used for functionalization, the binding sites in nonimprinted or imprinted mesoporous films could be considered as a homogeneous distribution.⁵

In this work, we followed the second Fick's law equivalent to describe the overall kinetic behaviors in the molecularly imprinted tubular mesoporous films.^{20,21}

2.1. Theoretical Formulation for the Molecularly Imprinted Tubular Mesoporous Film

Based on the above assumptions, small gas molecule diffusion-adsorption in TNT-imprinted mesoporous film with P6mm structure could be expressed by the formulas below:

$$\frac{\partial C^{av}}{\partial t} = \frac{D_{pore}}{L^2} \frac{\partial^2 C^{av}}{\partial y^2} - \frac{2\Gamma_{site}(y)(\rho k_{ads})}{r_{pore}} [(1-\theta)C^{av} - \theta(\phi K_{des})] \quad (1)$$

$$\frac{\partial \theta}{\partial t} = (\rho k_{ads}) [(1-\theta)C^{av} - \theta(\phi K_{des})] \quad (2)$$

To be solved, it should associate with a set of initial conditions ($t = 0$):

$$0 < y \leq 1: C^{av}(y, 0) = 0, \quad \theta(y, 0) = 0 \quad (3a)$$

$$y = 0: C^{av}(0, 0) = C_0^b, \quad \theta(0, 0) = 0 \quad (3b)$$

and boundary conditions ($t > 0$):

$$y = 0: C^{av}(0, t) = C_0^b \quad (4a)$$

$$y = 1: (\partial C^{av} / \partial y) = 0 \quad (4b)$$

The formulation in eqs 1-4 demonstrated that the overall kinetic exhibited by the MI-based mesoporous system at hand depended on a few parameters which incorporated kinetic or thermodynamic effectors. Note that D_{pore} was the diffusion coefficient of analyte, L was the half average length of the tubes, r_{pore} was the inner radius of mesopore, Γ_{site} was the surface concentration of nonimprinted or imprinted sites decorating the mesopore wall and $f(y)$ was the corresponding distribution function, C^{av} was the statistically average concentration of the analyte and C_0^b was the corresponding concentration under the saturated vapor pressure, k_{ads} and k_{des} was corresponding rate of constant of chemical adsorption and desorption ($k_{des} = K_{des}k_{ads}$, where K_{des} was desorption equilibrium constant), and ρ , ϕ were the regulatory factors to describe the molecular imprinting efficiency. Among these parameters, r_{pore} and C_0^b were known and the corresponding value was 5.6 nm, 10 ppb (TNT) and 180 ppb (DNT). However, the determination of other parameters required the curve fitting process. Note that, due to

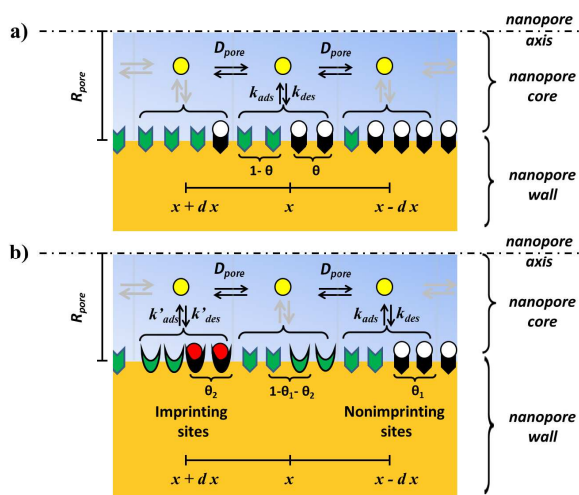


Figure 3. Schematic representation of 1D-diffusion-adsorption of analyte within the nonimprinted (a) and imprinted (b) mesoporous films.

the mesoporous film was fabricated by evaporation-induced self-assembly (EISA) method which usually resulted in small domains with randomly oriented mesoporous channels, the determination of the pore length was still a puzzle in this domain.²⁵ So in this paper, the combination of D_{pore} and L into one variable would be a feasible way for curve fitting.

2.2. Simulation and Fitting of the Experimental Curves

Using MATLAB software, we fitted the experimental curves base on the formulation above. During the fitting process, the values varied automatically in order to minimize the least-squared sum of residuals. The first experimental data was showed in Figure 4a corresponding to the nonimprinting mesoporous film. In this system, the regulatory factors of ρ , φ were used to describe the imprinting efficiency. So for the nonimprinting mesoporous film, ρ , φ were set to 1, indicating the non-adjustment ability. Also, due to the homogeneous distribution of binding sites, $f(y)$ was set to 1. The fitting curves of TNT and DNT in the similar figures showed that the solid lines matched excellently with the experimental data. The corresponding best-fitting parameters of TNT were: $D_{pore}/L^2=13s^{-1}$, $k_{ads}=8.44\times 10^8\text{ cm}^3\text{ mol}^{-1}\text{ s}^{-1}$, $k_{des}=0.0017s^{-1}$. And the ones of DNT were: $D_{pore}/L^2=35s^{-1}$, $k_{ads}=4.69\times 10^6\text{ cm}^3\text{ mol}^{-1}\text{ s}^{-1}$, $k_{des}=0.0014s^{-1}$. Comparing the parameter of k_{ads} between TNT and DNT, the former had the larger value or the larger binding affinity that mainly due to more electron-deficient property. Whereas, owing to the higher vapor concentration of DNT, it finally had the comparable quenching efficiency to TNT.

The second experimental data in Figure 4b were recorded the same as previous but in the system of TNT-imprinted mesoporous film. Again, the fitting curve matched excellently with the experimental data. The best-fitting parameters of TNT were: $D_{pore}/L^2=13s^{-1}$, $k_{ads}=8.44\times 10^8\text{ cm}^3\text{ mol}^{-1}\text{ s}^{-1}$, $k_{des}=0.0017s^{-1}$, $\rho=1$, $\varphi=1.4$. And the ones of DNT were: $D_{pore}/L^2=35s^{-1}$, $k_{ads}=4.69\times 10^6\text{ cm}^3\text{ mol}^{-1}\text{ s}^{-1}$, $k_{des}=0.0014s^{-1}$, $\rho=0.4$, $\varphi=2.86$. Clearly, molecular imprinting was a powerful strategy to modulate the binding strength of the trace explosive TNT and DNT binding to the binding sites lining along the mesopore walls. Actually, in this task, the using of the apparent parameters: $k_{app-ads}=\rho k_{ads}$, $k_{app-des}=\varphi k_{des}$ would be a better

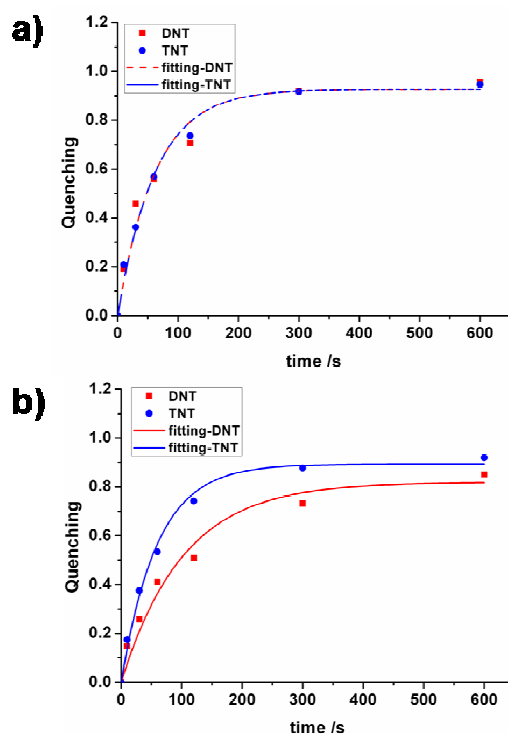


Figure 4. Kinetic and fitting results for trace explosive TNT and DNT detection based on nonimprinted (a) and imprinted mesoporous films (b). The best-fitting parameters are as follows: (a) TNT: $D_{pore}/L^2=13s^{-1}$, $k_{ads}=8.44\times 10^8\text{ cm}^3\text{ mol}^{-1}\text{ s}^{-1}$, $k_{des}=0.0017s^{-1}$, $\rho=1$, $\varphi=1$; DNT: $D_{pore}/L^2=35s^{-1}$, $k_{ads}=4.69\times 10^6\text{ cm}^3\text{ mol}^{-1}\text{ s}^{-1}$, $k_{des}=0.0014s^{-1}$, $\rho=1$, $\varphi=1$; for (b) TNT: $D_{pore}/L^2=13s^{-1}$, $k_{ads}=8.44\times 10^8\text{ cm}^3\text{ mol}^{-1}\text{ s}^{-1}$, $k_{des}=0.0017s^{-1}$, $\rho=1$, $\varphi=1.4$; DNT: $D_{pore}/L^2=35s^{-1}$, $k_{ads}=4.69\times 10^6\text{ cm}^3\text{ mol}^{-1}\text{ s}^{-1}$, $k_{des}=0.0014s^{-1}$, $\rho=0.4$, $\varphi=2.86$.

description of chemical adsorption and desorption rate. In TNT-imprinted mesoporous films, the apparent parameters for TNT were: $k_{app-ads}=8.44\times 10^8\text{ cm}^3\text{ mol}^{-1}\text{ s}^{-1}$, $k_{app-des}=0.0024s^{-1}$ and DNT were: $k_{app-ads}=1.88\times 10^6\text{ cm}^3\text{ mol}^{-1}\text{ s}^{-1}$, $k_{app-des}=0.004s^{-1}$. Evidently, by comparing these two kinds of films, in MI-based system where TNT molecules acted as the template, the rate of chemical adsorption was not affected but the rate of desorption increased. Whereas, when the TNT-imprinted system was used to detect its analog DNT, both of the two parameters varied greatly, for example, the value of $k_{app-ads}$ decreased about 60% and a significant increase (186%) occurred to $k_{app-des}$. Actually, this was the expected property because the nature of molecular imprinting was a well-established technique to mimic antibody functions.⁹ So in this way, we proved the validity of our constructed physicomathematical model. Indeed, by well controlling the imprinting efficiency, we might precisely control the diffusion-adsorption behaviors of the analytes in the pore channels and thus the overall sensing behaviors.

To conclude this section, we found that our above results were perfectly matched with the expectation through the established physicomathematical modeling. Based on the simple fitting procedure, some useful parameters such as the chemical adsorption/desorption rate could also be achieved. Whereas, for the better evaluating the MIP systems and further optimizing the sensor performance, it was essential to examine the role of the series of parameters of the ways to control the

overall kinetic and thermodynamic behaviors of analytes in the MIP systems.

3. The Examination of the Role of Each Parameter in MIP System

Small molecules diffusion in MIP systems is a complex process. As described above, the sensor performance (sensitivity and selectivity) was determined by a series of parameters. In order to extract the main factors that controlled the sensor performance and examine their ways to modulate the sensing behaviors, we needed to have a detail discussion on each parameter.

Sensitivity and selectivity were the two key performance parameters for sensor application. In our work, the above factors were divided into four groups: the structure factor, the distribution factor, the combination strength factor, and the molecular imprinting factor. In these factors, it was easy to find that the structure factor (pore size effect for selective sensing was excluded) and distribution factor were directly associated with the sensor sensitivity, whereas, the other two factors heavily determined the sensor selectivity. So in this section, the discussion was divided into two parts. Note that, for all the simulations in this work, the values of the corresponding parameters were mainly derived from Figure 4 for the approximation to the real system.

3.1 Sensitivity

In the part, we focused on the first two factors: the structure factor (pore length, pore size) and the distribution factor (the surface concentration and distribution of the binding sites), and examined their ways to modulate the sensing behaviors. Indeed, the ensuring theoretical views were greatly useful for they could be served as educated bases in several different conditions that enabled a broad discussion. Herein, in our discussion, three conditions: $k_{ads}/k_{des}=10$, 1 and 0.1 were used to represent the entire probable binding modes between the binding sites and analytes. Based on these three conditions, a comprehensive and deep understand on each parameter could be obtained.

In the first part, we examined the relationship between the parameter of pore length and sensor sensitivity. Commonly, the duration time for an analyte with a diffusion coefficient D (effective one or real one) to reach the far end of a tube with the length L was $T_{diff}=L^2/D$. Clearly, by shortening the pore length, the diffusion time of molecule inside the pore channel would be greatly shortened. As shown in Figure 5A1-3, at a first glance, all the three figures showed the similar sensing behaviors, where curve 3 had the best sensing sensitivity owing to the shortest pore length. In Figure 5A1, when the pore length was quite large, both curves 1 and 2 had the poor sensing. Even though the pore length of curve 2 was tenth of curve 1, the sensing capability improved little. However, when the pore length further reduced to one-tenth, the sensing capability of curve 3 improved significantly, indicating that in this case, the modulation of the sensor sensitivity via the change of pore length was associated with the primary pore length. Also, in Figure 5A2, the three curves showed the similar sensing behaviors. Whereas, due to the large desorption rate where $k_{ads}/k_{des}=1$, the maximum sensing value in curve 3 was almost the half in comparison with that in Figure 5A1. Moreover, when the rate of desorption was further increased where $k_{ads}/k_{des}=0.1$ in Figure 5A3, the sensing capability could also be well modulated even when the value of pore length was quite large. In conclusion this part, we found that the pore length was

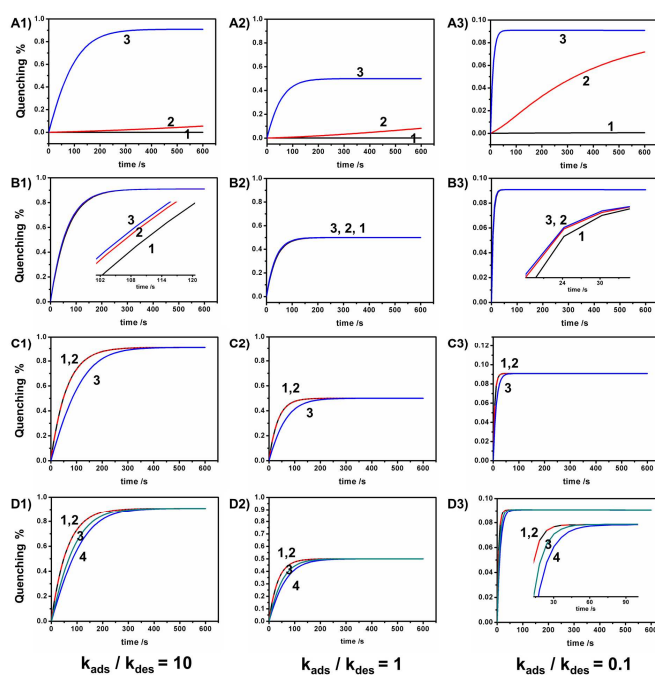


Figure 5. Dependence of the sensor sensitivity on various parameters: pore length (A), pore size (B), the surface concentration of binding sites (C), and the distribution function of binding sites inside the pore wall surface (D). Data for the simulations correspond to the following fixed parameters:³⁷ (A1-A3) $k_{ads}C_0^b=0.015$, $2\Gamma_{site}/(C_0^b r_{pore})=1000$, $f(y)=1$, $\rho=\phi=1$, $D_{pore}/L^2=0.001$, $L_1=10L_2=100L_3$, where $K_{des}=0.1$ for (A1), $K_{des}=1$ for (A2), and $K_{des}=10$ for (A3); (B1-B3) $k_{ads}C_0^b=0.015$, $K_{des}=0.1$, $f(y)=1$, $\rho=\phi=1$, $D_{pore}(r_1)/L^2=65.49$, $2\Gamma_{site}/(C_0^b r_1)=1120$, $D_{pore}(r_2)/L^2=89.13$, $2\Gamma_{site}/(C_0^b r_2)=560$, $D_{pore}(r_3)/L^2=98.92$, $2\Gamma_{site}/(C_0^b r_3)=373$, $r_1=5$ nm, $r_2=10$ nm, $r_3=15$ nm, where $K_{des}=0.1$ for (B1), $K_{des}=1$ for (B2), and $K_{des}=10$ for (B3); (C1-C3) $k_{ads}C_0^b=0.015$, $f(y)=1$, $\rho=\phi=1$, $D_{pore}/L^2=0.001$, $2\Gamma_{site}(1)/(C_0^b r_{pore})=1$, $\Gamma_{site}(1)=0.01\Gamma_{site}(2)=0.001\Gamma_{site}(3)$, where $K_{des}=0.1$ for (C1), $K_{des}=1$ for (C2), and $K_{des}=10$ for (C3); (D1-D3) $k_{ads}C_0^b=0.015$, $D_{pore}/L^2=70$, $\rho=\phi=1$, $2\Gamma_{site}(1)/(C_0^b r_{pore})=2\Gamma_{site}(2)/(C_0^b r_{pore})=1$, $2\Gamma_{site}(3)/(C_0^b r_{pore})=2\Gamma_{site}(4)/(C_0^b r_{pore})=10000$, $f_1(y)=f_3(y)=3.4\exp(-2.15y)-0.4$; $f_2(y)=f_4(y)=1$, where $K_{des}=0.1$ for (D1), $K_{des}=1$ for (D2), and $K_{des}=10$ for (D3).

indeed an important factor to modulate the sensor performance, whereas, the modulation ability was closely associated with the binding modes between the binding sites and analytes.

Furthermore, we focused on the parameter of pore size. Currently, numerous works had been performed on selective sensing analytes based on the pore size effect. However, in our discussion, this case had been excluded and the pore size r_{pore} was larger than the dimension of analytes. Pay attention to the equation 1, it was easy to find that the parameter of diffusion coefficient D_{pore} was closely associated with the pore size. Herein, we used the Higdon and Muldowney equation to express their relationship, where β was the ratio between the molecule and pore size:²⁹

$$\frac{D_{pore}}{D_0} = 1 + \frac{9}{8} \beta \ln \beta - 1.56034\beta + 0.528155\beta^2 + 1.91521\beta^3 - 2.81903\beta^4 + 0.270788\beta^5 + 1.10115\beta^6 - 0.435933\beta^7 \quad (5)$$

As shown in Figure 5B, in all the three figures, though the mesopore size varied from 5nm, to 10 and 15nm, the sensor performances were essentially the same, indicating that in the

mesopore region, the parameter of pore size was not the major factor to modulate the sensor sensitivity.

In the same way, we explored the parameter of the surface concentration of binding sites of the way to influence the sensor sensitivity. As shown in Figure 5C1-3, when the surface concentration was low, all the curve 1 and curve 2 had almost the same sensing behaviors. However, only when the value was large enough $\Gamma_{site}(3)=1000\times\Gamma_{site}(1)$, the sensor performance would be slightly modulated to have a poorer sensing, indicating the surface concentration was also not the major factor to modulate the sensor sensitivity.

In general, there were two available pathways to decorate the pore wall surface: grafting method and co-condensation method. Each method made a different binding sites distribution. Commonly, the grafting method had the advantage that the starting silica phase could be retained, but it always led to a non-homogeneous distribution and pore blocking effect. Whereas, for co-condensation method, the binding sites were generally more homogeneous distributed and pore blocking would not be a problem. So for a clear comparison, we simulated their sensing behaviors. In the simulation process, the diffusion-adsorption of analytes within the pore was always treated as a one-dimensional problem and the distribution density was a function of space coordinate. In our discussion, the distribution function for co-concentration method was assumed as $f(y)=1$. Whereas, for the function based on grafting method, due to centralized distribution near the pore mouth and sparse in the inner of binding sites, to enable a discussion, a function: $f(y)=3.4\exp(-2.15y)-0.4$ was supposed to fit for this kind of distribution.

Under the assumption, as shown in Fig. 5D1-3, when the surface concentration was low, the mesoporous film with different distributions had almost the same sensing behavior. However, only when the surface concentration increased 10000 times, the differential sensing appeared where the film with the distribution function of $f(y)=3.4\exp(-2.15y)-0.4$ had the better sensor sensitivity. Nevertheless, the difference between the two distributions was still quite small, indicating that the parameter of the distribution of binding sites in the pore wall surface was also not the major factor to modulate the sensor sensitivity.

To conclude this part, based on the theoretical discussion on the four parameters (pore length, pore size, the surface concentration and distribution of binding sites) of the ways to modulate the sensor sensitivity, we finally found that the parameter of pore length was the most important factor to influence the diffusion-adsorption behavior of analyte in MIP system and thus efficiently controlled the sensor performance.

The above result was encouraging and pushed us to have a further investigation on the macro-mesoporous systems where the addition of macropore was actually a facile way to reduce the pore length and so increased the mass transport and easier accessibility to the binding sites. In our previous work, on the basis of the combination of colloidal and mesophase templating, a general and effective approach for the preparation of macro-mesoporous films had been developed for trace explosive sensing.⁹ The sensing results proved the hierarchical porous film had the better sensing capability than mesopores film. In fact, in this kind of macro-mesoporous system, the parameters that modulate the sensor performance showed a complex multi-relationship. To have a theoretical discussion on the relationship between the pore structure and sensor performance, a physicomathematical model in macro-mesoporous system was generated for further discussion.

3.2. Theoretical Formulation for the Molecularly Imprinted Macro-Mesoporous Film

Firstly, before the foundation of the formulation, for the sake of simplifying the complex models, some reasonable assumptions should be made:

(i) During the synthesis process of the ordered array with FCC (face-centered cubic) structure, the defects were unavoidable. Herein, for the simplification, the defects were neglected.

(ii) The final inverse opal structure had a good replication of the FCC structure as shown in Figure S2. The replication structure was consisted of series of periodic tetrahedral and octahedral gaps which had the ratio of 2. During the detection process, the analytes diffused into the two kinds of gaps. However, due to the quite complex structures of the gaps, they were not suitable for mathematical modeling. So for a simplification, the complex structures of tetrahedral and octahedral gaps were translated into the equivalent spheres. Note that, the equivalent spheres were considered as the maximum spheres that could be held in the tetrahedral or octahedral gaps. The corresponding value for tetrahedral gap was 0.225R, and for octahedral gap was 0.414R, where R was the diameter of the used colloidal particles. And the partition coefficient of binding sites in tetrahedral gaps was 24.33%.

Based on the above assumptions, small gas molecule diffusion-adsorption in MI-based macro-mesoporous films could be expressed by the formulas below:

Macropore:

$$\frac{\partial q}{\partial t} = \frac{D_{pore}}{H^2} \frac{\partial^2 q}{\partial y_1^2} \quad (6)$$

Mesopore:

$$\frac{\partial C^{av}}{\partial t} = \frac{D_{pore}}{L_{av}^2} \frac{\partial^2 C^{av}}{\partial y_2^2} - \frac{2\Gamma_{site}(y)(\rho k_{ads})}{r_{pore}} [(1-\theta)C^{av} - \theta(\phi K_{des})] \quad (7)$$

$$\frac{\partial \theta}{\partial t} = (\rho k_{ads}) [(1-\theta)C^{av} - \theta(\phi K_{des})] \quad (8)$$

To be solved, it should associate with a set of initial conditions ($t = 0$):

Macropore:

$$q(y_1, 0) = 0 \quad (9)$$

Mesopore:

$$C^{av}(y_2, 0) = 0, \quad \theta(y_2, 0) = 0 \quad (10)$$

and boundary conditions ($t > 0$):

Macropore:

$$y_1=0: q(0, t) = C_0^b \quad (11a)$$

$$y_1=1: \partial q(1, t) / \partial t = 0 \quad (11b)$$

Mesopore:

$$y_2=0, \quad C^{av}(0, t) = f(q) \quad (12a)$$

$$y_2=1, \quad \partial C^{av}(1, t) / \partial t = 0 \quad (12b)$$

Note that, H was the film thickness, L_{av} was the half average length of tube which was the function of the diameter of colloidal particles, mesopore size, and the thickness of wall. The corresponding detail descriptions were played in the supporting information. $f(q)$ was the concentration of analyte at the entrance of mesopore. When the film thickness was thin, due to the fast diffusion of analyte in macropore, $f(q)$ was close to C_0^b .

In this system, the corresponding equivalent sphere was determined by the diameter of colloidal particle. The average length of tube was the function of the diameter of colloidal particle, mesopore size, and the thickness of wall. Also the diffusion coefficient D_{pore} was associated with the pore size. Obviously, the multi-relationships between these parameters were really annoying problems. Nevertheless, we simulated the

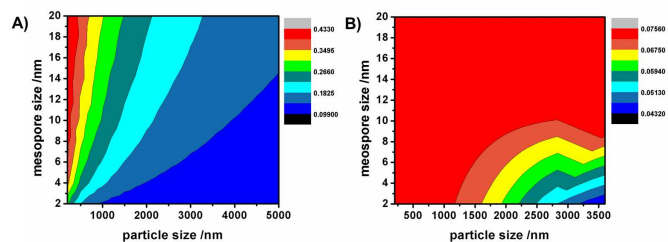


Figure 6. Variation of θ_{40s} as a function of parameters:³⁷ mesopore size and particle size. $k_{ads}C_0^b=0.015$, $f(y)=1$, $\rho=\varphi=1$, $2r_{site}/C_0^b=5.6 \times 10^{-4}$, where $K_{des}=0.1$ for (A), $K_{des}=1$ for (B).

relationships based on the physicomathematical models.

Figure 6a and 6b presented the contour plots of θ_{40s} in a (the diameter of colloidal particle R , mesopore size r_{pore}) diagram for the different binding modes: $k_{ads}/k_{des}=0.1$ and 1. θ_{40s} represented the local fraction of occupied binding sites at 40s. As shown in Figure 6a, θ_{40s} was larger at low R values since this corresponds to smaller colloidal particle and thus the shorter pore length, a fact that shortened the diffusion path, and for high value of r_{pore} , which corresponded to faster diffusion rate of molecule inside the pore channels. In addition, Figure 6a showed an interesting property of the macro-mesoporous systems. Indeed, at small R values, θ_{40s} became almost virtually independent of r_{pore} showing that under the condition of short pore length, the variation of the mesopore had no real influence on the sensor performance. Whereas, the variation of θ_{40s} with R and r_{pore} in Figure 6b showed the quite different sensing behavior. The dependence on r_{pore} was negligible when the parameter of R not very large. Only the size of colloidal particle reached to the micron dimension, the modulation behavior of r_{pore} could be observed. Nonetheless, due to the large desorption rate, the overall sensor performance varied in a small region. Based on the above simulations, we finally created the relationships between the sensor performance and porous structure and obtained the ways to modulate the sensing behaviors in macro-mesoporous systems.

3.3 Selectivity

Selectivity was another important factor to describe the sensor performance. In the MIP systems, extraction of the imprint molecules left a binding pocket with preorganized interaction sites and compatible size/shape to the imprinted molecules. The structure of functional monomer and cross-linker as well as the polymerization conditions directly determined the imprinting efficiency and thus their recognition properties. In this discussion, we wanted to have a theoretical and systemic exploration of the modulation behaviors of molecular imprinting and extracted the main factor to control the sensor selectivity.

As mentioned above, in our work, two regulatory factors of ρ , φ were used to describe the imprinting efficiency. Figure 7 presented the contour plot of R_{60s} in a (ρ , φ) diagram for the time at 60s. R_{60s} represented the selectivity where the value was derived by $Q_{imprinting}/Q_{nonimprinting}$ at 60s. The larger the value of R_{60s} , the better the discrimination ability or selectivity. As expected, R_{60s} was larger at large ρ values since this corresponded to the larger adsorption rate between the binding sites and analytes, a fact that improved the selective sensing, and for low values of φ , which corresponded to the smaller desorption rate. Also it was evidence from the figure that the dependence of R_{60s} on the parameter of φ was negligible when the parameter ρ was quite small. Only the value of $\ln(\rho)$

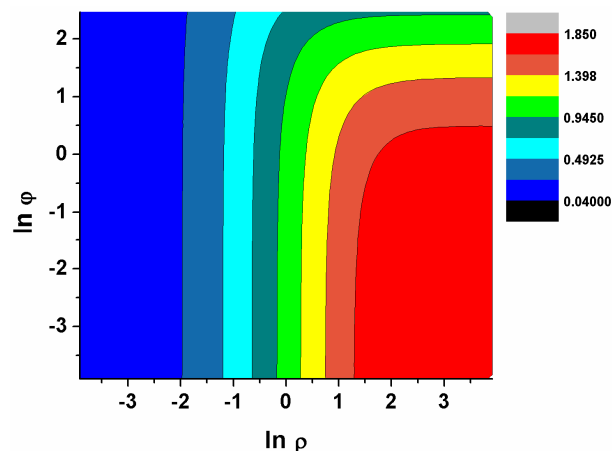


Figure 7. Variation of R_{60s} as a function of parameters:³⁷ ρ and φ . $k_{ads}C_0^b=0.02$, $K_{des}=0.085$, $D_{pore}/L^2=13$, $f(y)=1$, $2r_{site}/(C_0^b r_{pore})=1000$.

increased to 0, the modulation behavior of φ would appear at the large value. Based on the parameters for computation, the quenching of the nonimprinted mesoporous film was 54%, and so the largest value for R_{60s} was $1/0.54=1.85$. Indeed, in the region that $\ln(\rho) \in [1.5, 3.9]$ and $\log(\varphi) \in [-3.9, 0.5]$, R_{60s} has the largest value, indicating the best selectivity could be achieved in a wide range. In addition, by comparing the two parameters (ρ and φ) in Figure 6, we found that the parameter of ρ or the apparent rate of adsorption ($k_{app-ads}=\rho k_{ads}$) was more apparent to modulate the sensing selectivity.

Moreover, we further explored the way of molecular imprinting to modulate the diffusion-adsorption behaviors of target molecules inside the pore channels. In a real molecular imprinting system, various binding sites would exist in the same time. Actually, in our above discussion, the use of the two parameters of ρ and φ to represent the imprinting efficiency was one of the ways to simplify the model. However, to further understand the various binding sites in MIP systems of their ways to modulate the sensing behaviors, our above created models were not feasible. So based on the above consideration, new physicomathematical model was created below:

$$\frac{\partial C^{av}}{\partial t} = \frac{D_{pore}}{L^2} \frac{\partial^2 C^{av}}{\partial y^2} - \frac{2(1-\lambda)\Gamma_{site} k_{ads}}{r_{pore}} [(1-\theta_1 - \theta_2)C^{av} - \theta_1 K_{des}] - \frac{2\lambda\Gamma_{site} k'_{ads}}{r_{pore}} [(1-\theta_1 - \theta_2)C^{av} - \theta_2 K'_{des}] \quad (13)$$

$$\frac{\partial \theta_1}{\partial t} = k_{ads} [(1-\theta_1 - \theta_2)C^{av} - \theta_1 K_{des}] \quad (14)$$

$$\frac{\partial \theta_2}{\partial t} = k'_{ads} [(1-\theta_1 - \theta_2)C^{av} - \theta_2 K'_{des}] \quad (15)$$

To be solved, it should associate with a set of initial conditions ($t=0$):

$$0 < y \leq 1: C^{av}(y,0)=0, \theta_1(y,0)=0, \theta_2(y,0)=0 \quad (16a)$$

$$y=0: C^{av}(0,0)=C_0^b, \theta_1(0,0)=0, \theta_2(0,0)=0 \quad (16b)$$

and boundary conditions ($t > 0$):

$$y=0: C^{av}(0,t)=C_0^b \quad (17a)$$

$$y=1: (\partial C^{av} / \partial y) = 0 \quad (17b)$$

Note that, λ was the ratio of imprinted sites among all the binding sites, k_{ads} and k_{des} was the corresponding rate of constant of chemical adsorption and desorption of nonimprinted sites ($k_{des}=K_{des}k'_{ads}$, where K_{des} was desorption equilibrium

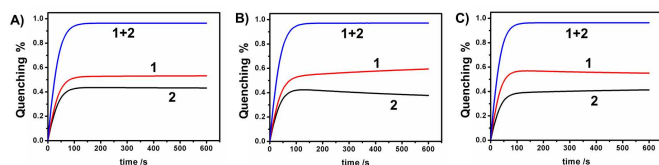


Figure 8. Dependence of the sensing behaviors on the variation of k'_{ads} and K'_{des} .³⁷ (A-C) $k_{ads}C_0^b=0.02$, $K_{des}=0.085$, $D_{pore}/L^2=13$, $2r_{site}/(C_0^b r_{pore})=1000$, $\lambda=0.5$, where $k'_{ads}=1.2k_{ads}$, $K'_{des}=0.8K_{des}$ for (A), $k'_{ads}=1.5k_{ads}$, $K'_{des}=0.8K_{des}$ for (B), and $k'_{ads}=1.2k_{ads}$, $K'_{des}=0.5K_{des}$ for (C).

constant), k'_{ads} and k'_{des} was the corresponding rate of constant of chemical adsorption and desorption of imprinted sites ($k'_{des}=K'_{des}k'_{ads}$).

In this discussion, we first explored the parameter λ of the way to modulate the sensing behavior. In general, the larger the ratio of the imprinted sites, the better the sensor selectivity. Whereas, in our simulation, when $k'_{ads}=1.1k_{ads}$, $K'_{des}=0.9K_{des}$, the variation of λ from 0.2 to 0.8 in Figure S3 made little difference (the increased ratio was only 0.56% at 60s) to the sensing, indicating the parameter of λ was not an important factor to control the sensor reactivity. In comparison, when $\lambda=0.5$, since the 10% variation of k'_{ads} and k'_{des} ($k'_{ads}=1.1k_{ads}$, $K'_{des}=0.9K_{des}$), the sensor selectivity was improved about 1.6% at 60s. The relative larger increased ratio demonstrated that the variation of the adsorption/desorption rate between the binding sites and analytes was a more effective way to modulate the sensor selectivity.

To further investigate the parameters of k'_{ads} and k'_{des} of their ways to modulate the diffusion-adsorption behaviors of analytes in the pore channels, three behaviors were discussed below ($\lambda=0.5$):

- (1) $k'_{ads} \uparrow 20\%$, $K'_{des} \downarrow 20\%$
- (2) $k'_{ads} \uparrow 50\%$, $K'_{des} \downarrow 20\%$
- (3) $k'_{ads} \uparrow 20\%$, $K'_{des} \downarrow 50\%$

As shown in Figure 8, all of the curves reached the equilibrium quickly. Also since the increase of k'_{ads} and decrease of K'_{des} , the imprinted parts showed the better sensitivity than the nonimprinted counterparts. In Figure 8A, when the parameters of k'_{ads} and K'_{des} had the same variation ratio, after the equilibrium, the sensing values in curve 1 and 2 kept steady. Whereas, for behavior 2 (Figure 8B), due to larger increasing ratio of adsorption rate, the sensing value in curve 1 would further slowly increase after the equilibrium, indicating the continual transfer of analytes from the nonimprinted sites to imprinted ones. Conversely, for behavior 3 (Figure 8C), the sensing curves had the inverse phenomenon. So based on the above simulations, the three figures clearly proved the molecular imprinting was a powerful strategy to modulate the diffusion-adsorption behaviors of analytes and thus the better control of the sensing behaviors.

3.4 Optimizing

Small molecules diffusion in MIP systems is a complex process. Indeed, the sensor performance (sensitivity and selectivity) was determined by a series of parameters which played the cooperative or adverse roles. Whereas, based on our discussions, in the molecularly imprinted tubular mesoporous systems, we found that the parameters of pore length L , and the parameter of ρ or the apparent rate of chemical adsorption $k_{app-ads}=\rho k_{ads}$ were the key factors to modulate the sensor sensitivity and selectivity. So in the following discussion, we explored the

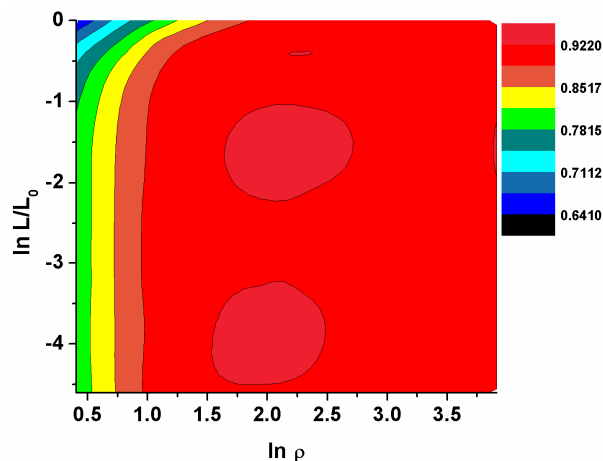


Figure 9. Variation of θ_{60s} as a function of parameters:³⁷ ρ and L/L_0 . $k_{ads}C_0^b=0.02$, $K_{des}=0.085$, $D_{pore}/L^2=13$, $f(y)=1$, $2r_{site}/(C_0^b r_{pore})=1000$, $\varphi=1$, $L/L_0 \in [0.01, 1]$.

relationships between two parameters (L , ρ) and the sensing performance. As shown in Figure 9, it was a contour plot of θ_{60s} in a (L/L_0 , ρ) diagram. As expected, θ_{60s} was larger at large ρ since this corresponded to the larger adsorption rate, and for low values of L/L_0 which corresponded to the shorter pore length and thus shortened the diffusion path. Moreover, the most important finding was the existence of the optimum region. When the two parameters stayed in the optimum region where $\ln(\rho) \in [1.6, 2.7]$, $\ln(L/L_0) \in [-2.2, -1.1]$ or the region where $\ln(\rho) \in [1.5, 2.5]$, $\ln(L/L_0) \in [-4.75, -3.25]$, the sensor with the best sensitivity and selectivity could finally be achieved. This useful information guided us for the design and fabrication of new chemosensors with higher performance in the future work.

Conclusions

In this work, two general and suitable physicomathematical models have been developed to provide a quantitative and general description of the fine and complex interplay between the diffusion and adsorption of small gas molecules occurring in the molecularly imprinted meso- and macro-mesoporous films. First, we proved the validity and suitability of the physicomathematical model by the experiments where trace explosive TNT and DNT detection was carried out in the TNT-imprinted mesoporous films with P6mm structure. Furthermore, based on the theoretical and numerical formulations, the roles of the related parameters (pore size, pore length, surface concentration, distribution of binding sites, the rate constants of chemical adsorption/desorption between the binding sites and analytes, and the imprinting efficiency) on the modulation of sensor sensitivity and the parameters were elucidated. Based on simulations, we found that the pore length and the apparent rate of adsorption were the most important factors to influence the sensitivity and selectivity of sensor, respectively. After the optimization of both parameters, a sensor with good sensitivity and selectivity could be achieved. These developed models in our work offered us useful information and guideline for design and fabrication of chemosensors with improved performance. Moreover, we believe that our models could be easily modified and expanded to other fields such as catalysis and separation, etc.

Acknowledgements

We gratefully acknowledge the financial support from the National Science Foundation of China (no. 21025311, 21121004, 21261130581 and 91027016), Ministry of Education (2011Z01014), MOST Program (2011CB808403, 2013CB-834502) and the transregional project (TRR61).

Notes and references

Key Lab of Organic Optoelectronics & Molecular Engineering

Department of Chemistry, Tsinghua University, Beijing, 100084 (China).

E-mail: LGT@mail.tsinghua.edu.cn

Electronic Supplementary Information (ESI) available: [details of any supplementary information available should be included here]. See

DOI: 10.1039/b000000x/

- 1 M. Antonietti and G. A. Ozin, *Chem.-Eur. J.* 2004, **10**, 28-41.
- 2 Z. Y. Yuan and B. L. Su, *J. Mater. Chem.* 2006, **16**, 663-677.
- 3 A. Thomas, F. Goettmann and M. Antonietti, *Chem. Mater.* 2008, **20**, 738-755.
- 4 Y. Wan and D. Zhao, *Chem. Rev.* 2007, **107**, 2821-2860.
- 5 F. Hoffman, M. Cornelius, J. Morell and M. Fröba, *Angew. Chem. Int. Ed.* 2006, **45**, 3216-3253.
- 6 D. Lin, X. Zhang, X. Cui and W. Chen, *RSC Adv.*, 2014, **4**, 27414-27421.
- 7 H. Pang, Y. Piao, L. Xu, Y. Bao, C. Cui, Q. Fu and Z. Li, *RSC Adv.*, 2013, **3**, 19802-19806.
- 8 H. Fan, Y. Lu, A. Stump, S. Reed, T. Baer, R. Schunk, V. Perez-Luna, G. Lopez and C. Brinker, *Nature*, 2000, **405**, 56-60.
- 9 W. Zhu, S. Tao, C. Tao, W. Li, C. Lin, M. Li, Y. Wen and G. Li, *Langmuir*, 2011, **27**, 8451-8457.
- 10 K. Mosbach, *Trends Biochem. Sci.* 1994, **19**, 9-14.
- 11 G. Wulff and A. Sarhan, *Angew. Chem. Int. Ed.* 1995, **34**, 1812-1832.
- 12 K. Shea, *J. Trends Polym. Sci.* 1994, **2**, 166-173.
- 13 L. Chen, S. Xu and J. Li, *Chem. Soc. Rev.*, 2011, **40**, 2922-2942.
- 14 M. J. Whitcombe, I. Chianella, L. Larcombe, S. A. Piletsky, J. Noble, R. Porter and A. Horgan, *Chem. Soc. Rev.*, 2011, **40**, 1547-1571.
- 15 B. Dirion, Z. Cobb, E. Schillinger, L. I. Anderson and B. Sellergren, *J. Am. Chem. Soc.*, 2003, **125**, 15101-15109.
- 16 M. Etienne, A. Quach, D. Grosso, L. Nicole, C. Sanchez and A. Walcarius, *Chem. Mater.* 2007, **19**, 844-856.
- 17 E. Johannessen, G. Wang and M. O. Coppens, *Ind. Eng. Chem. Res.* 2007, **46**, 4245-4256.
- 18 H. Alsyouri, O. C. Gobin, A. Jentys and J. A. Lercher, *J. Phys. Chem. C* 2011, **115**, 8602-8612.
- 19 R. Krishna, *J. Phys. Chem. C* 2009, **113**, 19756-19781.
- 20 C. Amatore, *Chem.-Eur. J.* 2008, **14**, 5449-5464.
- 21 C. Amatore, A. Oleinick, O. V. Klymenko, C. Delacote, A. Walcarius and I. Svir, *Anal. Chem.* 2008, **80**, 3229-3243.
- 22 C. Amatore, N. D. Mota, C. Sella and L. Thouin, *Anal. Chem.* 2007, **79**, 8502-8510.
- 23 J. Michaelis and C. Bräuchle, *Chem. Soc. Rev.*, 2010, **39**, 4731-4740.
- 24 A. Zürner, J. Kirstein, M. Döblinger, C. Bräuchle, T. Bein, *Nature*, 2007, **450**, 705-709.
- 25 B. Rühle, M. Davies, T. Lebold, C. Bräuchle and T. Bein, *ACS Nano*, 2012, **6**, 1948-1960.
- 26 B. Cohen, F. Sanchez and A. Douhal, *J. Am. Chem. Soc.*, 2010, **132**, 5507-5514.
- 27 F. Furtado, P. Galvosas, M. Goncalves, F. D. Kopinke, S. Naumov, F. Rodríguez-Reinoso, U. Roland, R. Valiullin and J. Kärger, *J. Am. Chem. Soc.*, 2011, **133**, 2437-2443.
- 28 Y. Fu, F. Ye, W. G. Sanders, M. M. Collinson and D. A. Higgins, *J. Phys. Chem. B* 2006, **110**, 9164-9170.
- 29 S. Lu, Z. Song and J. He, *J. Phys. Chem. B* 2011, **115**, 7744-7750.
- 30 O. Dudko, A. M. Berezhkovskii and G. H. Weiss, *J. Phys. Chem. B* 2005, **109**, 21296-21299.
- 31 A. Maldonado, C. Nicot, M. Wak, R. Ober, W. Urbach and D. Langevin, *J. Phys. Chem. B* 2004, **108**, 2893-2897.
- 32 S. W. Thomas, G. D. Joly and T. M. Swager, *Chem. Rev.*, 2007, **107**, 1339-1386.
- 33 D. T. McQuade, A. E. Pullen and T. M. Swager, *Chem. Rev.* 2000, **100**, 2537-2574.
- 34 M. E. Germain and M. J. Knapp, *Chem. Soc. Rev.*, 2009, **38**, 2543-2555.
- 35 Y. Salinas, R. M. Máñez, M. D. Macos, F. Sancenón, A. M. Costero, M. Parra and S. Gil, *Chem. Soc. Rev.*, 2012, **41**, 1261-1296.
- 36 S. Pramanik, C. Zheng, X. Zhang, T. L. Emge and J. Li, *J. Am. Chem. Soc.* 2011, **122**, 4153-4155.
- 37 The uint can be seen in the supporting information.